


Optical modulation of coherent phonon emission in optomechanical cavities

Cite as: APL Photonics **3**, 126102 (2018); <https://doi.org/10.1063/1.5040061>

Submitted: 14 May 2018 . Accepted: 17 September 2018 . Published Online: 18 October 2018

Jeremie Maire, Guillermo Arregui , Nestor E. Capuj, Martin F. Colombano, Amadeu Griol, Alejandro Martinez, Clivia M. Sotomayor-Torres, and Daniel Navarro-Urrios 



View Online



Export Citation



CrossMark

ARTICLES YOU MAY BE INTERESTED IN

[Single crystal diamond micro-disk resonators by focused ion beam milling](#)


APL Photonics **3**, 126101 (2018); <https://doi.org/10.1063/1.5051316>

[Invited Article: Enhanced four-wave mixing in waveguides integrated with graphene oxide](#)

APL Photonics **3**, 120803 (2018); <https://doi.org/10.1063/1.5045509>

[Inhibition of tunneling and edge state control in polariton topological insulators](#)

APL Photonics **3**, 120801 (2018); <https://doi.org/10.1063/1.5043486>




THE ADVANCED MATERIALS MANUFACTURER®

additive manufacturing epitaxial crystal growth cerium oxide polishing powder silver nanoparticles sputtering targets III-IV semiconductors CVD precursors europium phosphors

deposition slugs OLED Lighting spintronics solar energy osmium nanoribbons thin films chalcogenides AuNPs GDC Li-ion battery electrolytes 99.999% ruthenium spheres

endohedral fullerenes copper nanoparticles diamond micropowder CIGS MBE grade materials palladium catalysts flexible electronics beta-barium borate borosilicate glass dysprosium pellets YBCO pyrolytic graphite 3d graphene foam indium tin oxide mesoporous silica raman substrates sapphire windows tungsten carbide InGaAs barium fluoride carbon nanotubes lithium niobate scandium powder



gallium lump glassy carbon nanodispersions InAs wafers laser crystals ultra high purity materials MOFs surface functionalized nanoparticles organometallics quantum dot Al Si P S Cl Ar rare earth metals photovoltaics refractory metals MOCVD superconductors transparent ceramics ultra high purity silicon

American Elements opens up a world of possibilities so you can **Now Invent!**

Over 15,000 certified high purity laboratory chemicals, metals, & advanced materials and a state-of-the-art Research Center. Printable GHS-compliant Safety Data Sheets. Thousands of new products. And much more. All on a secure multi-language "Mobile Responsive" platform.

perovskite crystals yttrium iron garnet alternative energy h-BN gold nanocubes graphene oxide macromolecules photonics rhodium sponge fiber optics beamsplitters infrared dyes zeolites fused quartz metallocenes platinum ink buckyballs Ti-6Al-4V

Now Invent.™

The Next Generation of Material Science Catalogs

www.americanelements.com

Optical modulation of coherent phonon emission in optomechanical cavities

Jeremie Maire,^{1,a} Guillermo Arregui,¹ Nestor E. Capuj,^{2,3}
 Martin F. Colombano,^{1,4} Amadeu Griol,⁵ Alejandro Martinez,⁵
 Clivia M. Sotomayor-Torres,^{1,6} and Daniel Navarro-Urrios^{7,a}

¹*Catalan Institute of Nanoscience and Nanotechnology (ICN2), CSIC and BIST, Campus UAB, Bellaterra, 08193 Barcelona, Spain*

²*Depto. Física, Universidad de La Laguna, 38200 San Cristóbal de La Laguna, Spain*

³*Instituto Universitario de Materiales y Nanotecnología, Universidad de La Laguna, 38071 Santa Cruz de Tenerife, Spain*

⁴*Depto. Física, Universidad Autonoma de Barcelona, Bellaterra, 08193 Barcelona, Spain*

⁵*Nanophotonics Technology Center, Universitat Politècnica de València, 46022 València, Spain*

⁶*Catalan Institute for Research and Advances Studies ICREA, 08010 Barcelona, Spain*

⁷*MIND-IN2UB, Departament d'Electrònica, Facultat de Física, Universitat de Barcelona, Martí i Franquès 1, 08028 Barcelona, Spain*

(Received 14 May 2018; accepted 17 September 2018; published online 18 October 2018)

Optomechanical (OM) structures are well suited to study photon-phonon interactions, and they also turn out to be potential building blocks for phononic circuits and quantum computing. In phononic circuits, in which information is carried and processed by phonons, OM structures could be used as interfaces to photons and electrons thanks to their excellent coupling efficiency. Among the components required for phononic circuits, such structures could be used to create coherent phonon sources and detectors, but more complex functions remain challenging. Here, we propose and demonstrate a way to modulate the coherent phonon emission from OM crystals by a photothermal effect induced by an external laser, effectively creating a phonon switch working at ambient conditions of pressure and temperature and the working speed of which is only limited by the build-up time of the mechanical motion of the OM structure. We additionally demonstrate two other modulation schemes: modulation of harmonics in which the mechanical mode remains active but different harmonics of the optical force are used, and modulation to and from a chaotic regime. Furthermore, due to the local nature of the photothermal effect used here, we expect this method to allow us to selectively modulate the emission of any single cavity on a chip without affecting its surroundings in the absence of mechanical coupling between the structures, which is an important step toward freely controllable networks of OM phonon emitters. © 2018 Author(s). All article content, except where otherwise noted, is licensed under a Creative Commons Attribution (CC BY) license (<http://creativecommons.org/licenses/by/4.0/>). <https://doi.org/10.1063/1.5040061>

INTRODUCTION

Numerous technologies have been tapping in the vast potential arising from manipulating excitations, among which electrons and photons are two of the most widespread examples. However, to use phonons in a similar way remains challenging since their coherent creation, manipulation, and detection, being key elements for their practical use, prove difficult to realize. Due to the lack of discrete phonon transitions in solids at ambient conditions, major efforts have been deployed to generate coherent phonons. These phonon sources can be used for on-chip metrology and time-keeping¹ or mass/force sensing,² amongst other foreseen applications.³ Optomechanical (OM) crystals have

^aAuthors to whom correspondence should be addressed: jeremie.maire@icn2.cat and daniel.navarro@icn2.cat

become one of the most efficient way to coherently emit phonons. Whereas coherent phonons can be generated via short laser pulses,^{4–6} radiation pressure⁷ is the most common mechanism used in OM cavities to generate coherent vibrations at GHz frequencies^{1,8–10} via dynamical back-action induced self-oscillation or more recently stimulated Brillouin scattering in either waveguides or cavities.^{11–14} However, a cooperativity above unity is required, and thus only modes with high quality factors and large optomechanical coupling strength can reach the “phonon lasing” regime. Recently, a new scheme for coherent phonon creation was introduced to overcome these issues. The coherent mechanical emission is based on a thermal/free carrier self-pulsing (SP) limit cycle modulating the intracavity photon number and pumping a mechanical mode of the structure, thus creating a self-stabilized coherent phonon source with relaxed requirements for both the optical and mechanical modes.¹⁵ Furthermore, as phonons can efficiently couple to other information carrier such as photons and electrons, phononic circuits could be used as interfaces in information processing devices. In this context, sources alone are only one step toward this purpose as additional functions are required, among which the most commonly sought-after is the synchronization of different emitters. Previous studies have started tackling this issue,^{16–22} as a first step toward future synchronized networks. Nevertheless, the functionalities of the emitters themselves remain limited to single mode continuous emission.

Here, we propose a scheme to address a single cavity without affecting its surroundings and modulate its coherent phonon emission properties. We use external optical pumping to induce photothermal heating of the cavity which changes the optical response via the thermo-optic (TO) effect. Practically, the modulation is caused by the shift of the resonance due to the added energy, which enabled us to realize a static phonon switch and a periodic on/off modulation of phonon lasing. The coherent phonon emission itself is achieved through the SP limit cycle described in our previous work,^{15,23} whereas an external optical source is used for modulation. The OM cavity displays other interesting regimes, such as chaos,²⁴ which is attracting interest in various other systems such as memories, sensing, secure data communications, and switches,^{25,26} but also as a good test bed for studying more complex dynamics which result from a higher dimension parameter space or increasing the complexity of the non-linear system. One can also imagine an array of such OM cavities that can be coupled into a multichannel chaotic source and multiplexed into a single optical fibre. Similar regimes, and, in particular, chaos, have been reached before in micro-resonators by means of dynamical back-action from a continuous wave (CW) optical input.²⁷ In the present work, upon reaching these regimes by means of the SP limit cycle, we not only use the photothermal effect to change the emission properties of the OM cavity but we also demonstrate state modulation between these regimes. Finally, we suggest a way to extend this concept toward multi-states switches that can eventually be integrated in future networks of coupled oscillators.

MATERIALS AND METHODS

The OM crystal used in this study [Fig. 1(a)] is fabricated from a silicon-on-insulator wafer (resistivity $\rho \sim 1\text{--}10\ \Omega\ \text{cm}^{-1}$, p-doping of $\sim 10^{15}\ \text{cm}^{-3}$). The top silicon layer and buried oxide layer have thicknesses of 220 nm and 2 μm , respectively. The structures were patterned in a 100 nm thick PMMA resist layer with electron-beam lithography and transferred to the silicon layer by reactive ion etching. The oxide layer was subsequently removed with buffered hydrofluoric acid to release the OM crystal. The unit-cell consists of a Si square with two symmetric stubs in which a cylindrical hole is etched. The OM crystal consists of three sections, namely, a central cavity surrounded by two sets of 10 mirror cells. The nominal parameters of these mirror cells are $a = 500\ \text{nm}$, $r = 150\ \text{nm}$, and $d = 250\ \text{nm}$, where a is the pitch, r is the radius of the hole, and d is the stub length parallel to the central axis of the OM crystal. The central cavity comprises 12 unit cells in which a , r , and d are decreased in a quadratic way toward the center. The central part of the beam and the stubs have a width of 500 nm, and the whole device length is about 15 μm . The free-standing OM crystal is clamped on both ends to the Si layer, which is suitable for optical actuation. The detailed fabrication process and geometry have already been described.^{15,28}

The OM structures are characterized by evanescent light coupling into the cavity from a tapered fibre at room-temperature and atmospheric pressure.^{24,28} The driving laser is an infrared (IR) laser

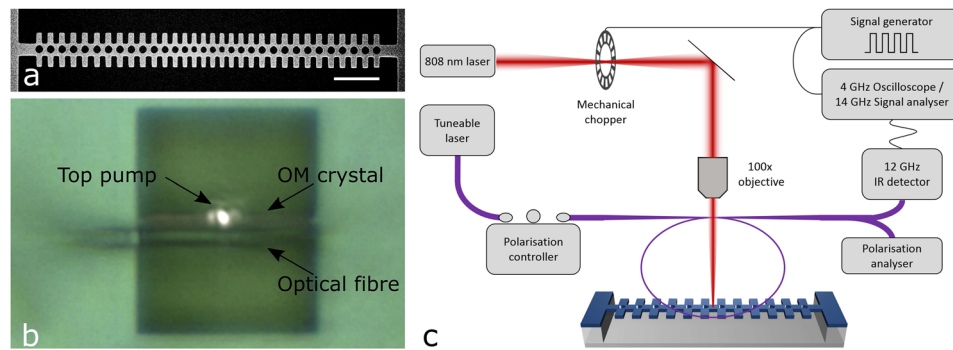


FIG. 1. **Experimental details.** (a) SEM image of an OM crystal, here in shape of a suspended Si nanobeam. Scale bar is 2 μm . (b) Optical image showing a top view of the OM crystal with the fibre below and the pump laser spot. The length of the nanobeam is 16.5 μm . (c) Schematic of the evanescent fibre coupling measurement system.

with tunable wavelength in the range of 1440–1640 nm and power up to 20 mW. The laser passes through a polarization controller before being coupled to a tapered microlooped fibre. The micro-loop is positioned approximately 200 nm away from the OM crystal, resting on an edge of the etched frame, as can be seen from Fig. 1(b). The evanescent field from the micro-loop excites the optical resonances of the OM crystal. The mechanical modes activated by the thermal Langevin force then modulate the transmission of the tapered fibre around its static value when the laser wavelength is inside an optical resonance of the OM crystal. The signal is then detected by a InGaAs detector of bandwidth 12 GHz and transmitted to a signal analyser with a bandwidth of 13.5 GHz. An 808 nm continuous-wave solid-state laser is used as an external optical pump to switch between the different states of the OM crystal. The wavelength has been chosen in the visible range for ease of alignment—see top pumping spot on the OM crystal in Fig. 1(b)—and for practical heating considerations in our experimental setup, i.e., to avoid overheating. The beam passes through a pinhole to reduce its diameter, and is then modulated by a mechanical chopper at 10 kHz, with a total on-off transition time of 8.5 μs . The beam is then focused on the OM crystal by a 100 \times microscope objective, as shown in Figs. 1(b) and 1(c). The temporal signals are acquired by an oscilloscope with 4 GHz bandwidth and a small mirror is used to split up part of the laser beam to trigger the acquisition.

We first characterize the basic optical and mechanical properties of the OM structure. For that purpose, we start by acquiring a low-power (0.2 mW) optical transmission spectrum which displays a number of resonances, shown as sharp dips in the spectrum of Fig. 2(a), superposed to the transmission of the fibre whose oscillations are associated with modes of the micro-loop. As the OM coupling coefficient is higher for low-order modes, we usually focus on the fundamental resonance, i.e., the resonance at the lowest wavelength, to excite mechanical vibrations. Increasing the optical input power results in a “saw-tooth” shaped transmission, as the resonant frequency is red-shifted due to the contribution of the thermo-optic (TO) effect,²⁹ an example of which is shown in red in Fig. 2(a). The mechanical spectrum is obtained by processing the transmitted optical signal with a spectrum analyser. The initial state corresponds to a large laser-cavity blue-detuning, i.e., the wavelength of the laser is shorter than the wavelength of the resonance, and then the driving wavelength is progressively increased. For a large detuning, i.e., low intracavity photon number, the thermal motion of string-like mechanical modes can be readout through Lorentzian peaks in the transmission spectra with quality factors on the order of 10^2 . Due to symmetry considerations,¹⁵ we focus on the second order (three anti-nodes) mechanical odd mode of frequency $\nu_{m,2} = 54$ MHz. Decreasing the detuning from the blue side leads to an increase in the intracavity photon number, eventually bringing the OM crystal into a SP limit cycle^{15,30–34} that modulates the intracavity photon number and thus the optical force drives the mechanical oscillator. Self-pulsing appears as a complicated nonlinear dynamics when the intracavity photon number is high enough (typically above a few 10^4) and stems from the interplay between the free-carrier dispersion (FCD) and the TO effect, which are the main source of nonlinearities in silicon resonators at 1.55 μm .²⁹ The increase in free carriers leads to a reduction

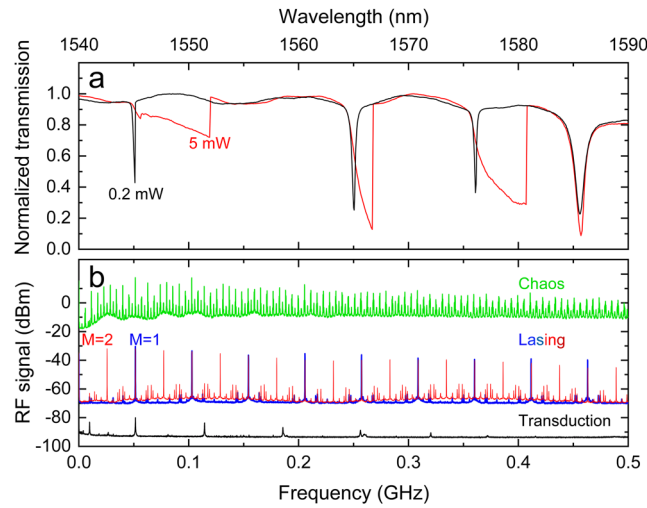


FIG. 2. **Optomechanical characterization.** (a) Spectra of the optical transmission normalized to its baseline. Optical resonances appear as sharp dips in the transmission spectrum acquired at low power, at which the thermo-optic effect is weak (black curve). The resonances in the spectrum acquired at high power (red curve) display an asymmetric shape characteristic of the thermo-optic effect. (b) Mechanical spectra for different regimes of the OM cavity, i.e., transduction of thermally activated modes (black), phonon lasing thanks to the 1st and 2nd harmonics of the optical force (blue and red curves, respectively) and chaos (green), from bottom to top, respectively. The spectra are shifted along the vertical axis for clarity.

of the refractive index³⁵ and therefore a blue-shift of the optical resonance, whereas an increase in temperature due to the thermo-optic effect has the opposite effect. The system can be modeled by a system of coupled equations linking the dynamics of the free-carrier density (N) and the temperature increase (ΔT),^{15,30,33}

$$\frac{dN}{dt} = -\frac{1}{\tau_{FC}}N + \beta n_0^2 \frac{hc^3}{n^2 \lambda_0 V_0^2}, \quad (1)$$

$$\frac{d\Delta T}{dt} = -\frac{1}{\tau_T}\Delta T + \alpha_{FC}Nn_0, \quad (2)$$

where n_0 is the intracavity photon number, h is the Planck constant, c is the speed of light, V_0 is the optical mode volume, and α_{FC} is defined as the rate of temperature increase per photon and unit free-carrier density. In the FCD [Eq. (1)],²³ β is the two-photon absorption coefficient¹⁶ and surface recombination is governed by a characteristic lifetime τ_{FC} . The TO effect [Eq. (2)] reflects the balance between the fraction of photons that are absorbed and transformed into heat due to free carrier absorption (FCA) and the heat dissipated to the surroundings of the cavity volume, which is governed by a characteristic thermal lifetime τ_T . As the driving wavelength is further increased, the frequency of the SP limit cycle increases until one of the higher harmonics of the optical force overlaps with the mechanical resonance and coherently excites the mechanical oscillator. Due to this optomechanical coupling, the SP receives feedback from the mechanical mode and the SP frequency stabilizes, matching a fraction of that of the mechanical mode, leading to its amplification and resulting in coherent, high-amplitude mechanical vibrations, qualified as phonon lasing.¹⁵ Increasing further the wavelength can lead to coherent activation of other mechanical states, two of which are shown in Fig. 2(b). Indeed, the blue, respectively, red, spectra of Fig. 2(b) (center) correspond to the cases in which the first, respectively, second, harmonics of the optical force coincide with the mechanical frequency. For specific values of the driving laser parameters, a chaotic regime can be reached,²⁴ a spectrum of which is shown in Fig. 2(b) (top). Further details on the self-pulsing mechanism are available in our previous work.¹⁵ Below, we explain the principle of the modulation mechanism, followed by our experimental observations and describe the characteristics of the phonon switch realised via the external pumping scheme.

RESULTS AND DISCUSSION

Modulation mechanism

To clarify the impact of the top-pump on the regimes available, we acquire two maps of RF spectra as a function of wavelength, one corresponding to the initial condition, i.e., without additional pumping [Fig. 3(a)] and a second with external pumping [Fig. 3(b)], both with a driving laser power of 10 mW. It is clear that the resonance displays similar regimes, including lasing regimes in which the mechanical mode is excited by different harmonics of the optical force, from the 5th to the 1st, as the driving wavelength increases (see details in Fig. 1 of the [supplementary material](#)), but shifted to longer wavelengths when additional pumping is introduced. To explain this observation, and the subsequent modulation experiments, let us first look at the “pump off” state. Scanning the laser wavelength from the blue-detuned side of an optical resonance, the thermo-optic effect produces a strongly asymmetric line shape, as shown in Fig. 2(a) and represented by a blue line in Figs. 3(c) and 3(d). During the experiment, the driving laser is fixed at a specific wavelength, which corresponds to one of the regimes of the structure, e.g., transduction, self-pulsing, phonon lasing, or chaos in Fig. 3(c). When activating the external optical modulation, the external pump acts as a source of energy for the OM crystal, hence increasing its temperature and enhancing the thermo-optic effect. From the observation of Figs. 3(a) and 3(b), this can be represented by a shift of the mean position of the resonance to longer wavelengths, as shown in Fig. 3(d) (see also Fig. 2 of the [supplementary material](#)). Comparatively, the driving wavelength in the fibre, which is already fixed, will be further away from the perfect resonant configuration. In the example given in Figs. 3(c) and 3(d), this brings the system to the SP regime (pump on) from the initial mechanical lasing regime (pump off). Hence, in the modulation experiments presented hereafter, the initial state (pump off) always corresponds to the regime requiring the highest driving wavelength, i.e., the largest detuning. When turning on the pump, the system then reverts to a state requiring, in principle, a shorter wavelength, i.e., smaller detuning. Note that the infrared excitation wavelength in the optical fibre is fixed during each experiment. Figure 4 of the [supplementary material](#) shows all the transitions that it is possible to achieve for a fixed power of the 808 nm top pump by varying the input laser wavelength. On the other hand, Fig. 5

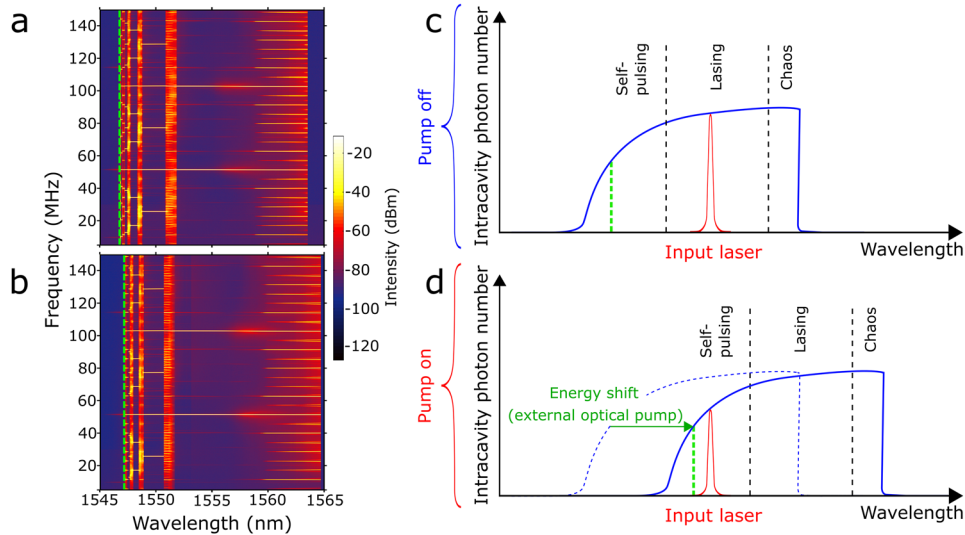


FIG. 3. Modulation mechanism. (a) Map of RF spectra as a function of wavelength, around a specific optical resonance, without external pumping. (b) Identical resonance recorded with external pumping switched on. A clear shift toward longer wavelengths is observed as compared to (a). The green dashed lines in all panels mark the onset of the SP regime. (c) Simplified diagram representing the change in regime of the OM cavity due to the effect of top-pumping. The resonance is shown as a function of wavelength. The asymmetry stems from the thermo-optic effect and the three regions within the resonance are given as an example. The driving laser is used to bring the system to the mechanical lasing regime. (d) The external optical pump is switched on, shifting the resonance to longer wavelengths. The driving laser remains at the same wavelength as in the “pump off” state, hence the change in the dynamics of the system.

of the [supplementary material](#) shows that, with different top pumping powers, it is possible to reach different states from a single starting point, in this case from a phonon lasing state excited by the 2nd harmonic of the optical force.

Theoretically, it should be possible to modulate the phonon emission properties of the OM crystal by a combination of positive and negative power pulses of the IR driving laser. However, two key difference emerge: (i) the modulation mechanism are different, as a power modulation of the IR laser modifies the number of photons in the cavity. The states accessible in the resonance are therefore changed too. The method presented here, however, plays on the number of free carriers and the temperature of the cavity, and the same regimes as without top pump remain available. (ii) The IR laser can be used to excite several OM cavities (not studied in this work) in which case a modification of this laser properties, such as the driving power, would affect all cavities regardless of their inter-coupling, whereas the method presented here affects only a single cavity in the absence of inter-coupling.

Phonon switch

After analysing the steady-state dynamical solution for both excitation schemes, we perform the modulation experiments. In all of them, the excitation laser is used to bring the system to the initial state, after which wavelength and power remain fixed, whereas the optical pump is used to trigger the modulation. We first drive the system, without external pumping, to the mechanical lasing regime at 54 MHz, the spectrum of which is displayed in Fig. 4(a) (top). The optical pump is then turned on, effectively switching off the mechanical lasing, as shown by the corresponding spectrum in Fig. 4(a) (bottom). To identify the two states with more precision, the temporal signals shown in Fig. 4(b) are examined. Whereas the on-state of the external pumping leads to a very weak modulation of the signal, the initial state shows a comb of harmonics of the main RF peak typical of the phonon lasing regime driven by SP, fully described in our previous work.¹⁵ Note that although Fig. 4(a) (bottom) shows the 54 MHz mechanical mode with low amplitude, we have also observed

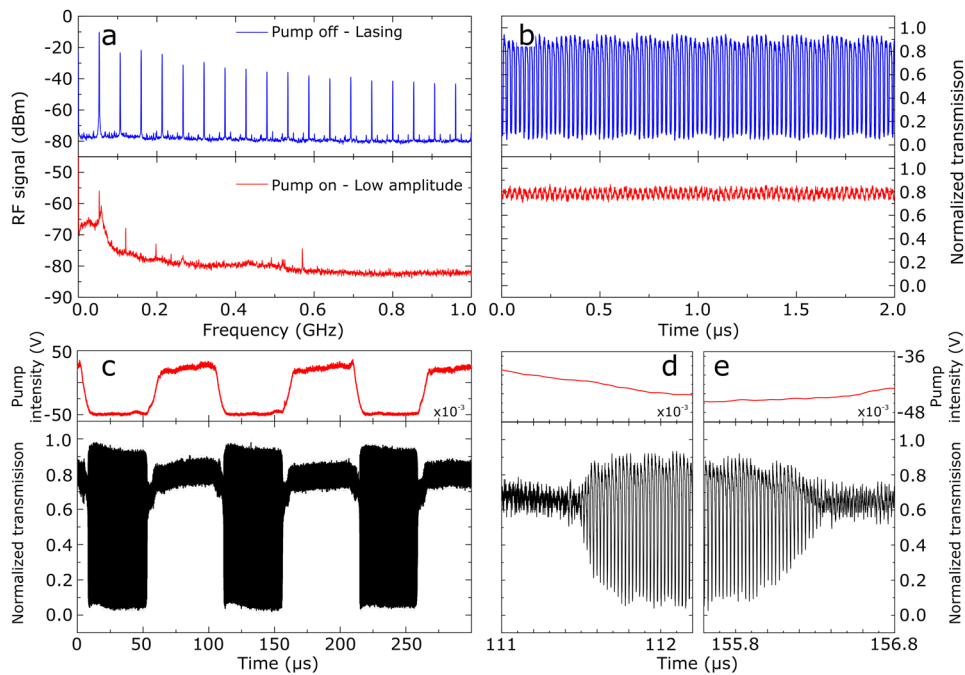


FIG. 4. Modulation of phonon emission. (a) RF spectra in the initial lasing regime (pump off, top) and in a low mechanical amplitude regime with self-pulsing (pump on, bottom). (b) Corresponding temporal signal for the lasing (top) and SP (bottom) regimes. (c) Large scale temporal signal displaying the external pumping signal (top) and the corresponding signal from the OM crystal. [(d) and (e)] Zoom on the temporal signals of the on \rightarrow off and off \rightarrow on transitions of the phonon switch, respectively.

the modulation between the lasing regime and a pump-on state in which the spectrum does not display anything except for the background noise (see video 1 of the [supplementary material](#)). With the on/off states clearly identified, we then focus on the modulation mechanism itself. For that purpose, we record high-resolution temporal signals of both the external optical pump and the signal from the OM structure, both shown in Fig. 4(c). The normalized transmission clearly shows a periodic signal with two distinct regions: a low amplitude signal when the external pump is on and high amplitude oscillations when the pump is off. The high amplitude oscillation is at the frequency of the mechanical mode, whereas in the low amplitude region, the frequency is unstable, as is characteristic of the SP regime.

Such a switch has two main characteristics: the modulation speed and the pump power required for modulation. The switching speed is discussed in the section titled Numerical results and the limiting factors are the chopper speed and the lifetime of the mechanical mode. Experimentally, we take a close-up look at the on/off transitions in Figs. 4(d) and 4(e), recorded at a repetition rate of 10 kHz. After a transition is initiated, we observe that approximately 200 ns are needed for the signal to stabilize in its new state.

To address the pump power required for modulation, we first monotonically increase the driving laser wavelength until phonon lasing is observed. Then, we increase the external pump power until we see, as in Fig. 4, that the modulation is stable by cycling the pump on and off. In this situation, the lowest pump power at which we observed modulation was 130 μW . This power is measured just after the microscope objective and represent the power needed by our experiment to induce modulation, and can be optimized by enhancing absorption of the incident power, as using the absorption coefficient of silicon³⁶ to estimate the total absorbed power yields a value of 1.7 μW for an driving power of 130 μW .

Numerical results

Once we ascertained the mechanism behind the modulation, we numerically integrate the equations of the system. They comprise the two coupled equations of self-pulsing (corresponding to the free carrier dispersion and the thermo-optic effect) linked to the equations of the mechanical resonator (displacement and velocity). The details of the model are given in our previous studies, in which we show that the experimental measurements are well reproduced.¹⁵ We modify the equations to include a source term that shifts the resonance by a fixed amount to represent the impact of the photo-thermal heating of the structure, i.e., the resonance shift in wavelength stemming from the sample heating due to the laser irradiation. The shift is ramped up from 0 to the desired value over 400 ns (smallest computationally available shift) with steps of 3 ps.

We start the simulation with a small cycle in which no mechanical oscillation is observed and the transmission is constant. This situation is shown in blue in Fig. 5(a), in particular, in the projection of the initial solution on the $(u-\Delta T)$ plane, which does not display mechanical oscillations. We then shift the resonance until we reach a stable phonon lasing regime, shown by the red cycle. In that regime, the system displays high-amplitude oscillations, as shown on the $(u-\Delta T)$ plane and the shape of the cycle is also displayed on the $(N-\Delta T)$ plane. In Fig. 5(b), we calculate the corresponding transmission and plot the windowed fast Fourier transform (FFT), using windows of 370 ns (~ 20 periods of the mechanical mode) and shifting the window center linearly. The transition is initiated at $t = 10 \mu\text{s}$, and a zoom on the transition is shown in inset. We can see from the windowed FFT that the stable mechanical frequency (f_{mec}) is reached rapidly, i.e., in less than 1 μs . Additionally, the transition to the transmission displaying the SP oscillations occurs faster than the time required for the SP oscillation to complete one cycle. At that time, the mechanical mode is already coherently driven but has not yet reached its full amplitude of oscillations. Indeed, the time it takes for this mode to reach a steady-state in amplitude depends on the lifetime of the mechanical mode. Hence, the transition time is influenced by three time scales, either experimental or intrinsic: (i) the transition time of the pump, here linked to the chopper's cutoff of the laser beam, (ii), the lifetime of the mechanical mode, which in our case is on the order of 10 μs , and (iii) the photo-thermal heating time, i.e., the time taken for a photon to be absorbed and converted to heat, which is on the order of 10 ps.^{37–39} This latter time sets a lower physical limit in modulating the coherent phonon emission via photo-thermal absorption, regardless of the mechanical mode. In our case, the modulation time is mainly

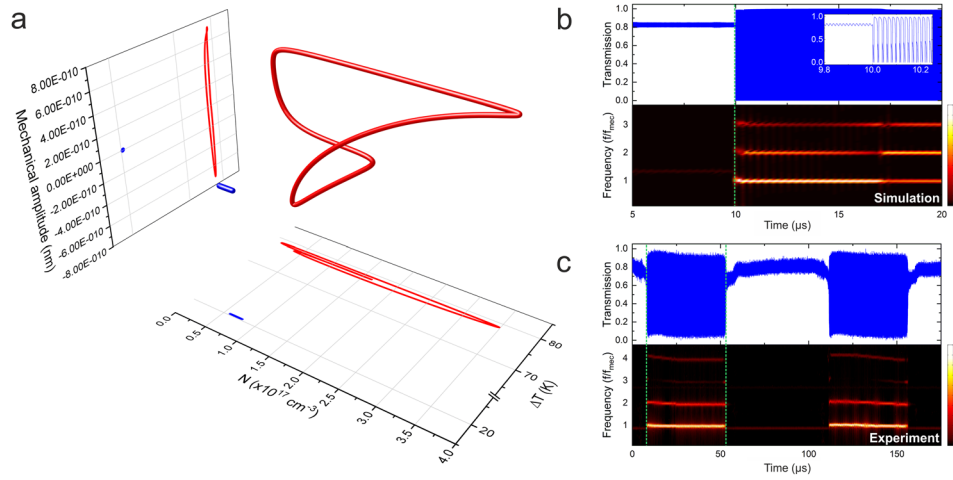


FIG. 5. **Numerical results.** (a) 3D representation of the photon number versus the temperature increase versus the mechanical amplitude. The blue and red dots delimit the first (SP) and last (phonon lasing) limit cycle, respectively. The projections of these two cycles are shown with blue and red lines, respectively. (b) Calculated transmission and frequency spectrum as a function of time. The transmission change from a near-constant value to the periodic oscillation (phonon lasing regime) at the frequency of the mechanical mode. (c) Experimental transmission and extracted frequency spectrum as a function of time. The green dashed lines denote a phonon lasing region.

limited by the chopper and the mechanical mode. Although the lifetime of the mechanical mode is much longer than the transition, the amplitude does not need to reach its steady-state value to observe the onset of phonon lasing. Similarly, a large portion of the beam cut-off time by the chopper is spent on cutting part of the beam that does not contribute to the photothermal effect and thus to the modulation. Hence the transition is faster than these two characteristic times. To check the validity of our calculations, we repeat the same process with the experimental data in Fig. 5(c). The observation is similar to that of the simulation, with the dynamics quickly stabilizing at the mechanical frequency after the transition, which confirm our hypothesis on the modulation speed. A faster transition of the pump states using a top pump laser at 405 nm (see Figs. 7–9 of the [supplementary material](#)) gives us some additional information concerning the transitions. Whereas there is no change to activate the high-amplitude signal (see Fig. 8 of the [supplementary material](#)), we observe a difference for the decay of the mechanical mode, i.e., when the pump is switched on. The use of a chopper in this case masks the dynamics, in which the mechanical mode, coupled to the optical signal, gradually decrease over a time of several microseconds. More details are given together with Figs. 7–9 of the [supplementary material](#).

Switching between other regimes

A number of regimes are available in the OM crystal under study. Therefore, we investigate the additional switching possibilities available. In the modulation scheme presented before, the first harmonic of the optical force (in the SP regime) is used to bring the system to mechanical lasing. In a previous work, we showed that it is possible to use higher harmonics to bring the same mechanical mode to lasing as well.¹⁵ Hence, we perform modulation experiments between the 1st ($M = 1$) and 2nd ($M = 2$) harmonic driving of the mechanical mode (Fig. 6). We observe that this transition occurs instantaneously, i.e., there is no discontinuity in the mechanical lasing temporal trace, whereas the period of the total transmission is divided by 2, as shown in inset of Fig. 6. In this case, the mechanical mode is already active. Hence, the transition only involves the SP phenomena, i.e., thermo-optic and free carrier dispersion. The absence of a visible transition region indicates that the change occurs much faster than the relatively long period of the limit cycle, which indicates that the photothermal dynamics is indeed faster than the other time scales in our experiment. Switching between other harmonics of the optical force has also been observed both with the red top pump ($M = 3 \leftrightarrow M = 4$) and the blue top pump ($M = 2 \leftrightarrow M = 3$) (see Figs. 3 and 5 of the [supplementary material](#), respectively).

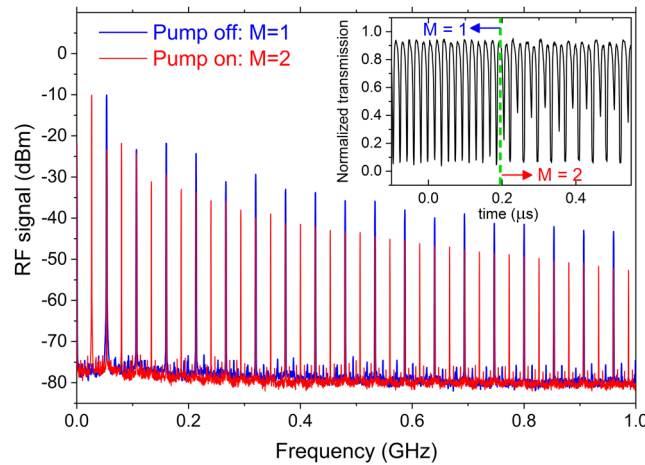


FIG. 6. **Modulation of harmonics.** RF spectra in the phonon lasing regime driven by the first ($M = 1$) and second ($M = 2$) harmonics of the optical force (Inset) Temporal signal of the transition between the pump off state ($M = 1$) and the pump on state ($M = 2$).

More interestingly, we focus on modulation involving a chaotic state. Figures 7(a) and 7(b) show the spectra and temporal signals in the chaotic (top) and phonon lasing (bottom) regimes. The chaotic regime is a complex dynamical solution to the multi-dimensional system of equations governing the nanobeam dynamics. We have shown before that this system of equations comprises two equations for the self-pulsing regime, linked to the free-carrier population and the average cavity temperature increase, and two first-order equations for each mechanical mode, governing the displacement and speed of motion, respectively.²⁴ The numerical model developed to explain this dynamics showed that the mechanical motion remains coherent, even if the SP dynamics have turned chaotic.

To investigate chaos modulation, the system is initially put in the chaotic state and the external optical pumping is then applied. In a similar way to the phonon lasing modulation, under external pumping the system reverts back to a state requiring shorter driving wavelength, i.e., a larger blue

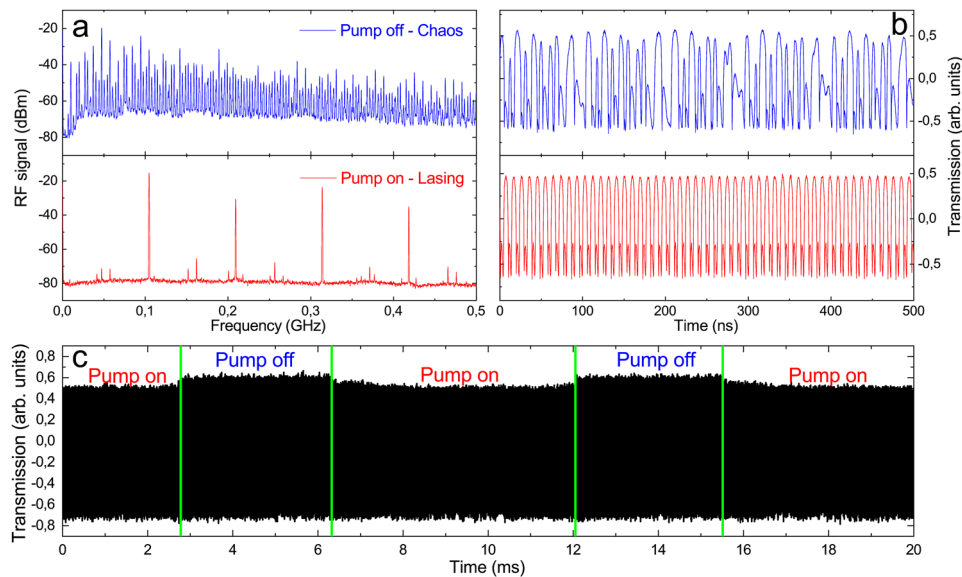


FIG. 7. **Chaos-Lasing modulation.** (a) RF spectra in the initial chaotic regime (pump off, top) and in the phonon lasing regime (pump on, bottom). (b) Corresponding temporal signals for the chaotic (top) and lasing (bottom) regimes. (c) Large scale temporal signal displaying both on and off regions of the optical pumping.

detuning, in this case phonon lasing. Due to the complex nonlinear signals, it is difficult to precisely characterize the modulation speed, but from inspection of the transitions in Fig. 7(c), the exclusively optical nature of the modulation involved, given that the mechanical mode stays active in both the on and off states, enables extremely fast modulation, i.e., fast enough for the transition to occur within one period of the mechanical vibration.

CONCLUSIONS

We have presented in this work a proof of concept of modulation of phonon emission, one of the crucial functions to implement phononic circuitry, as well as examples of modulation between different states of the optomechanical system. We have shown the possibility to locally address a single OM cavity and modulate its coherent phonon emission. This feature will become increasingly important in the future, as the number of phonon emitters per unit area will increase. In addition, this method is tailored specifically for the phonon lasing scheme of this work and is valid at ambient temperature and pressure conditions. The power required to modulate the phonon emission is less than 3% of that used to reach the phonon lasing regime. In this work, CW pumping is required to keep a given state active. However, it is possible in principle to combine this technique with multistable systems, in which short pulses will be sufficient to change between two or more dynamical states. Bistability, for example, has already been demonstrated in this type of OM cavities for both power and wavelength.²⁴ Finally, a very promising route is to intercouple two or more similar OM cavities either with mechanical or optical weak links and investigate the switching functions demonstrated in this work in the context of synchronized oscillators, which is the focus of our next study. Therefore, this work is a promising step toward the realisation of phononic circuit functions with OM crystals by bringing a new addition to the few OM components already available, namely, phonon sources and memories, as well as opening the path toward multi-state memories in multi-stable regions.²⁴

SUPPLEMENTARY MATERIAL

[Supplementary material](#) is separated in two main sections corresponding to the red and blue top pumps, respectively. The first section starts with details about the regimes inside the optical resonance followed by the impact of the top pump on the optical resonance. Then, results are presented concerning the regimes achievable for a constant top pump power at different driving wavelengths, and for different top pump powers at a fixed driving wavelength. This experiment is then repeated with the blue top pump. Finally, based on temporal traces acquired with the blue top pump, the transition between phonon lasing and transduction is discussed in more details when the transition time of the pump is much faster than the dynamics of the system.

ACKNOWLEDGMENTS

This work was supported by the European Commission FET Open project PHENOMEN (No. H2020-EU-713450) and the Spanish MINECO project PHENTOM (No. FIS2015-70862-P). The ICN2 is funded by the CERCA programme, the Generalitat de Catalunya, and supported by the Severo Ochoa programme of the Spanish MINECO Grant No. SEV-2013-0295. D.N.U. and M.F.C. gratefully acknowledge the support of a Ramón y Cajal postdoctoral fellowship (No. RYC-2014-15392) and a Severo Ochoa studentship, respectively. The authors thank F. Alzina for fruitful discussions.

¹ M. Aspelmeyer, T. J. Kippenberg, and F. Marquardt, *Rev. Mod. Phys.* **86**, 1391 (2014).

² X. L. Feng, C. J. White, A. Hajimiri, and M. L. Roukes, *Nat. Nanotechnol.* **3**, 342 (2008).

³ Y. Pennec, V. Laude, N. Papanikolaou, B. Djafari-rouhani, M. Oudich, S. El Jallal, J. C. Beugnot, J. M. Escalante, and A. Martínez, *Nanophotonics* **3**, 413 (2014).

⁴ C. Thomsen, J. Strait, Z. Vardeny, H. J. Maris, J. Tauc, and J. J. Hauser, *Phys. Rev. Lett.* **53**, 989 (1984).

⁵ R. Merlin, *Solid State Commun.* **102**, 207 (1997).

⁶ P. Ruello and V. E. Gusev, *Ultrasonics* **56**, 21 (2015).

⁷ E. Verhagen, S. Deleglise, S. Weis, A. Schliesser, and T. J. Kippenberg, *Nature* **482**, 63 (2012).

⁸ T. J. Kippenberg and K. J. Vahala, *Science* **321**, 1172 (2008).

⁹ D. Navarro-Urrios, J. Gomis-Bresco, S. El-jallal, M. Oudich, A. Pitanti, N. E. Capuj, A. Tredicucci, F. Alzina, A. Griol, Y. Pennec, B. Djafari-Rouhani, A. Martínez, and C. M. S. Torres, *AIP Adv.* **4**, 124601 (2014).

- ¹⁰ D. Navarro-Urrios, J. Gomis-Bresco, F. Alzina, N. E. Capuj, P. D. García, M. F. Colombano, E. Chavez-Angel, and C. M. Sotomayor-Torres, *J. Opt.* **18**, 094006 (2016).
- ¹¹ M. Merklein, I. V. Kabakova, T. F. S. Büttner, D.-Y. Choi, B. Luther-Davies, S. J. Madden, and B. J. Eggleton, *Nat. Commun.* **6**, 6396 (2015).
- ¹² T. Baehr-jones, R. Shi, and D. J. Blumenthal, *Nat. Photonics* **10**, 432 (2016).
- ¹³ J. Li, H. Lee, T. Chen, and K. J. Vahala, *Opt. Express* **20**, 20170 (2012).
- ¹⁴ N. T. Otterstrom, R. O. Behunin, E. A. Kittlaus, Z. Wang, and P. T. Rakich, *Science* **360**, 1113 (2018).
- ¹⁵ D. Navarro-Urrios, N. E. Capuj, J. Gomis-Bresco, F. Alzina, A. Pitanti, A. Griol, A. Martinez, and C. M. Sotomayor-Torres, *Sci. Rep.* **5**, 15733 (2015).
- ¹⁶ A. Pikovsky, M. Rosenblum, and J. Kurths, *Synchronization: A Universal Concept in Nonlinear Science* (Cambridge University Press, 2003).
- ¹⁷ G. Heinrich, M. Ludwig, J. Qian, B. Kubala, and F. Marquardt, *Phys. Rev. Lett.* **107**, 043603 (2011).
- ¹⁸ M. Zhang, G. S. Wiederhecker, S. Manipatrani, A. Barnard, P. McEuen, and M. Lipson, *Phys. Rev. Lett.* **109**, 233906 (2012).
- ¹⁹ M. Bagheri, M. Poot, L. Fan, F. Marquardt, and H. X. Tang, *Phys. Rev. Lett.* **111**, 213902 (2013).
- ²⁰ M. H. Matheny, M. Grau, L. G. Villanueva, R. B. Karabalin, M. C. Cross, and M. L. Roukes, *Phys. Rev. Lett.* **112**, 014101 (2014).
- ²¹ E. Gil-Santos, M. Labousse, C. Baker, A. Goetschy, W. Hease, C. Gomez, A. Lemaître, G. Leo, C. Ciuti, and I. Favero, *Phys. Rev. Lett.* **118**, 063605 (2017).
- ²² M. Zhang, S. Shah, J. Cardenas, and M. Lipson, *Phys. Rev. Lett.* **115**, 163902 (2015).
- ²³ D. Navarro-Urrios, N. E. Capuj, M. F. Colombano, P. D. García, M. Sledzinska, F. Alzina, A. Griol, A. Martinez, and C. M. Sotomayor-Torres, in *International Conference on Transparent Optical Networks (ICTON)* (IEEE, 2016), pp. 4–7.
- ²⁴ D. Navarro-Urrios, N. E. Capuj, M. F. Colombano, P. D. García, M. Sledzinska, F. Alzina, A. Martinez, and C. M. S. Torres, *Nat. Commun.* **8**, 14965 (2017).
- ²⁵ M. Peil, L. Larger, and I. Fischer, *Phys. Rev. E* **76**, 045201 (2007).
- ²⁶ F. Monifi, J. Zhang, S. K. Özdemir, B. Peng, Y. Liu, F. Bo, F. Nori, and L. Yang, *Nat. Photonics* **10**, 399 (2016).
- ²⁷ T. Carmon, M. C. Cross, and K. J. Vahala, *Phys. Rev. Lett.* **98**, 167203 (2007).
- ²⁸ J. Gomis-Bresco, D. Navarro-Urrios, M. Oudich, S. El-Jallal, A. Griol, D. Puerto, E. Chavez, Y. Pennec, B. Djafari-Rouhani, F. Alzina, A. Martínez, and C. M. Sotomayor Torres, *Nat. Commun.* **5**, 4452 (2014).
- ²⁹ P. E. Barclay, K. Srinivasan, and O. Painter, *Opt. Express* **13**, 801 (2005).
- ³⁰ T. J. Johnson, M. Borselli, and O. Painter, *Opt. Express* **14**, 817 (2006).
- ³¹ L. Zhang, Y. Fei, Y. Cao, X. Lei, and S. Chen, *J. Opt. Soc. Am. B* **31**, 201 (2014).
- ³² J. Yang, T. Gu, J. Zheng, M. Yu, G. Lo, D. Kwong, and C. W. Wong, *Appl. Phys. Lett.* **104**, 061104 (2014).
- ³³ W. H. P. Pernice, M. Li, and H. X. Tang, *Opt. Express* **18**, 18438 (2010).
- ³⁴ Y. Deng, F. Liu, Z. C. Leseman, and M. Hossein-zadeh, *Opt. Express* **21**, 4653 (2013).
- ³⁵ Q. Xu and M. Lipson, *Opt. Lett.* **31**, 341 (2006).
- ³⁶ C. Schinke, P. C. Peest, J. Schmidt, R. Brendel, K. Bothe, M. R. Vogt, I. Kröger, S. Winter, A. Schirmacher, S. Lim, H. T. Nguyen, and D. Macdonald, *AIP Adv.* **5**, 067168 (2015).
- ³⁷ S. H. Lee and J. Mech, *Sci. Technol.* **19**, 1378 (2005).
- ³⁸ M. Harb, R. Ernstorfer, T. Dartigalongue, C. T. Hebeisen, R. E. Jordan, and R. J. D. Miller, *J. Phys. Chem. B* **110**, 25308 (2006).
- ³⁹ Y. Liu and H. K. Tsang, *Appl. Phys. Lett.* **90**, 211105 (2007).